

Large Diameter Bulk Crystal Growth and Scintillation Characterization of Thallium-Based Ternary Halide Crystals for Detection and Imaging

Rastgo Hawrami (Xtallized Intelligence, Inc.)

ABSTRACT

Scintillators cover an important wide range of applications in detection and imaging. In this paper we are presenting growth and performance results of several advanced large diameter thallium-based ternary halide crystals are presented. Intrinsic crystals of TlMgCl_3 , TlCaCl_3 , TlCaBr_3 , and $\text{TlCa}(\text{Cl},\text{Br})_3$, as well as europium-doped TlCa_2Br_5 and $\text{TlCa}(\text{Cl},\text{Br})_3$ are melt-grown by the Bridgman method. These compounds have high Z_{eff} due to thallium and expected to have high physical densities. The best crystal quality and energy resolution (FWHM) at 662 keV are observed for intrinsic TlMgCl_3 . The primary decay constants for these compounds are in the range of 0.45 to 0.55 μs . All of these compounds have proportional or linear response to γ -ray above 100 keV.

INDEX KEYWORDS

Gamma-ray detectors. Inorganic scintillators. Intrinsic scintillators. High detection efficiency. Ternary compounds. Thallium-based scintillators.

INTRODUCTION

Advances in high energy physics depend on the advancement in materials research. Research in scintillators for particle detectors in high energy physics is pushed by a need for new, high-performance particle scintillation detectors with better energy resolutions, higher light yields, high densities, fast decay times, and are radiation hard [1]. Along with these desirable properties, these materials must also be stable, low cost, as well as easy to produce in large volumes and massive quantities.

Some of the most studied radiation detector materials currently available in market are inorganic binary compound scintillators [2]. Ternary compounds that are based on these binary compounds are usually formed by adding metal cations. Initial examples of these ternary compounds are online [2], with many more ternary compounds published in recent years. Many these recent advances in materials study for radiation sensors, particularly the latest discovery of high-density thallium-based inorganic scintillation crystals, is spurred by a necessity to improve isotope identification capability, for example, for homeland security applications. These new materials also possess many of the required properties for detection materials in high energy physics applications and research. Continuous search for improved scintillation materials for better radiation detection is important, since an ideal scintillator for such applications has yet to be discovered.

Recently high detection efficiency Tl-based scintillation crystals have attracted good attention from worldwide scintillator researchers. These compounds have been investigated and

very promising initial results have been published, for example Ce-doped Tl_2LaCl_5 (TLC) [3] as well as *intrinsic* (i.e., not doped) TlMgCl_3 (TMC) and TlCaI_3 (TCI) [4]. These new compounds are of high densities ($< 5 \text{ g/cm}^3$), bright (light yields between 31,000 and 76,000 ph/MeV for 662 keV photons), fast decay times (36 ns (89%) for TLC; 46 ns (9%) for TMC; 62 ns (13%) for TCI), and moderate melting points (between 500 and 700°C). As seen further in the published results, Tl-based scintillators such as the ones previously mentioned have promising properties desirable for high energy physics as well as homeland security applications [3-10].

At high photon energy, when pair production interactions producing electron-positron pairs dominates, material properties such as radiation length X_0 , nuclear interaction length λ_I , and Moliere radius R_M characterize the amount of matter is traversed by charged particles produced as well as the spread of the electromagnetic showers for these related interactions. Materials with high Z constituents tend to have lower values of X_0 , λ_I , and R_M . Tables 1 show that oxide-based scintillators have the overall lowest

Table 1. X_0 , λ_I , and R_M values for scintillators listed in Table 1, along with NaI, CsI, BGO, LSO, and PbWO_4 for comparison.

X_0 (cm)	Scintillator	R_M (cm)	Scintillator	λ_I (cm)	Scintillator
0.89	PbWO_4	1.98	PbWO_4	20.3	PbWO_4
1.09	BGO	2.05	LSO	20.6	LSO
1.14	LSO	2.16	BGO	22.3	BGO
1.49	TlCaI_3	2.83	TlMgCl_3	29.4	TlMgCl_3
1.64	TlMgCl_3	3.05	TlCaI_3	32.8	TlCaI_3
1.86	CsI	3.54	CsI	38.0	CsI
2.59	NaI	4.09	NaI	42.1	NaI

values of X_0 , λ_I , and R_M , followed by TMC and TCI two representative (intrinsic) Tl-based ternary compounds, hence these Tl-based scintillators can be presented as candidate materials in high energy physics applications.

Following the results of previously studied compounds, Xtallized Intelligence, Inc. (XI, Inc.) has grown several large (> 16 -mm) diameter single bulk crystals of intrinsic and doped thallium-based ternary compound scintillators for high energy physics applications. These compounds include $\text{Tl}_a\text{M}_b\text{X}_c$, where A is metal, such as Mg or Ca, and X are halogens, such as Cl, Br, or I, with $a = 1$ or 2, $b = 1$ or 2, and $c = 3$ or 5. For high energy physics purposes, ideal physical dimensions of a detection material should accommodate at least $20 X_0$ (e.g., 17.8 cm (7 inches) for PbWO_4 , 32.8 cm (12.9 inches) for TlMgCl_3). Therefore, to obtain amenable crystals, large diameter growth of crack-free, single crystals must be accomplished. In the following sections the growth and crystal analysis of intrinsic crystals of TlMgCl_3 , TlCaCl_3 , TlCaBr_3 , and $\text{TlCa}(\text{Cl,Br})_3$, as well as europium-doped TlCa_2Br_5 and $\text{TlCa}(\text{Cl,Br})_3$ are presented.

EXPERIMENTAL METHODS

Each of the Tl-based ternary compounds were grown by

Table 2. Starting binary compounds and the resulting ternary compounds.

Starting Binary Compounds	Dopant	Ternary Compounds
$\text{TlCl} + \text{MgCl}_2$		TlMgCl_3
$\text{TlCl} + \text{CaCl}_2$		TlCaCl_3
$\text{TlCl} + \text{CaBr}_2$		TlCaBr_3
$\text{TlCl}_x + \text{TlBr}_{1-x} + \text{CaCl}_x + \text{CaBr}_{2-x}$		$\text{TlCa}(\text{Cl,Br})_3$
$\text{TlCl} + 2 \text{CaBr}_2$	EuBr_2	$\text{TlCa}_2\text{Br}_5\text{:Eu}$
$\text{TlCl}_x + \text{TlBr}_{1-x} + \text{CaCl}_x + \text{CaBr}_{2-x}$	EuCl_2 or EuBr_2	$\text{TlCa}(\text{Cl,Br})_3\text{:Eu}$

stoichiometric mixing of the respective binary compounds. Table 2 shows the binary compounds, dopants, and the resulting ternary compounds. Starting materials of the highest available purity were purchased from US-based chemical vendors. For each targeted ternary compound, stoichiometric amounts of the binary compounds and dopants were purified if necessary using different techniques of purifications and loaded into a freshly cleaned and baked quartz ampoule. Material loading was conducted inside an inert glove box with an argon atmosphere. Using a turbo vacuum pump, the loaded ampoule was dehydrated, if necessary, and then sealed in a high vacuum. The ampoule was placed in a two-zone vertical furnace for growth with the Bridgman method. The top zone of the furnace was set a few degrees above the melting temperature of the compound to ensure a complete melt. The bottom zone was set a few degrees below the crystallization temperature for the compound. The growth was conducted at a rate of 15-25 mm/day. After the crystallization was completed, the ampoule was cooled down 75-150°C/day to room temperature. The crystal was then retrieved from the growth ampoule and samples were extracted by slicing the boule with a diamond wire saw. Lapping and polishing were conducted using Al₂O₃ and/or SiC polishing pads with mineral oil as lubricant.

Sample characterization was done by encapsulating a sample in a hermetic packaging or by immersing a sample in mineral oil contained in a quartz cup surrounded with diffuse reflectors (Teflon tape and Gore ® pad) for a quick test. For the latter measurement configuration, the quartz cup was coupled to a Hamamatsu R6231-100 photomultiplier tube (PMT) with BC-630 silicone optical coupling compound. Gamma-ray spectroscopy with ¹³⁷Cs was done to determine the energy resolution of each scintillator at 662 keV. Other gamma ray sources, such as ²⁴¹Am, ¹³³Ba, ²²Na, and ⁶⁰Co were used to determine both energy resolutions and relative light yield (i.e., non-proportionality) data. Decay time was determined by using a CAEN DT5720 digitizer to collect the PMT anode signals, which were then analyzed offline.

RESULTS AND ANALYSIS

TiMgCl₃

Started with Ø16-mm growths, several good quality transparent Ø1" TiMgCl₃ crystal boules were then grown at XI, Inc., two of which are shown in Fig. 1. Thermal stress that occurred during ampoule cooling produced a crack visible in the first boule, which measured approximately 10 cm in length (Fig. 1a). Single transparent crack free crystal samples of TiMgCl₃, however, were successfully obtained from this boule (Fig. 1a). With better quality

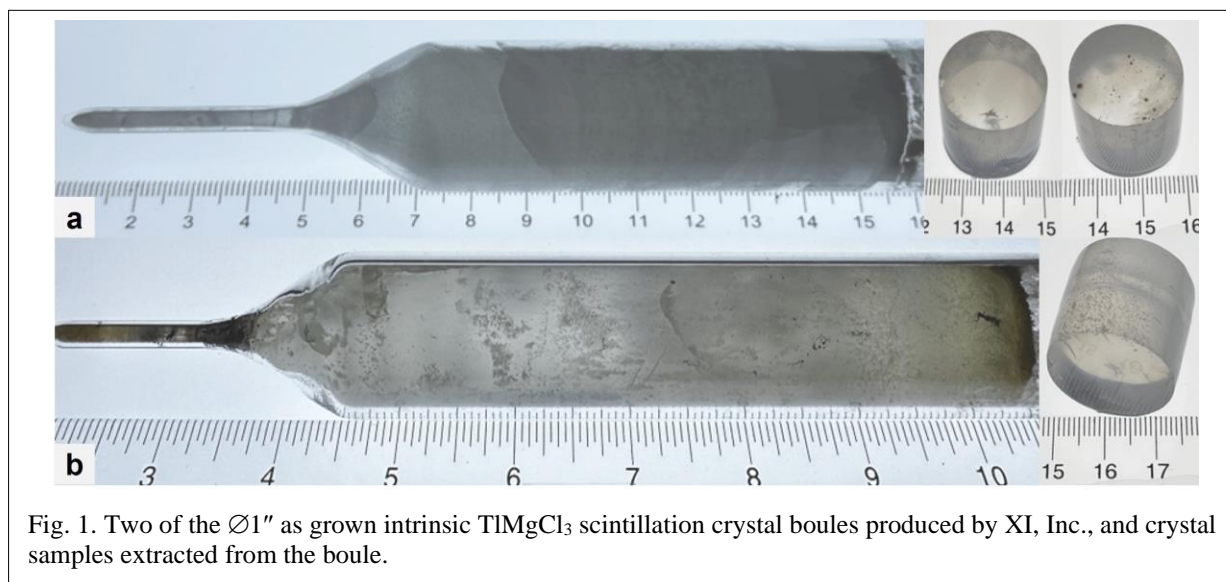


Fig. 1. Two of the Ø1" as grown intrinsic TiMgCl₃ scintillation crystal boules produced by XI, Inc., and crystal samples extracted from the boule.

purified materials, the second boule, which measures approximately 18 cm was grown single, transparent crack free. Mechanical stress due to improper crystal processing produced a chip visible in the obtained sample (Fig. 1b). Regardless of these aforementioned imperfections, growth of $\varnothing 1''$ TiMgCl_3 single crystal boules with sizeable lengths is achievable.

Fig. 2a shows one of the polished TiMgCl_3 crystal samples from the first boule. The temporal profile of the $5 \times 7 \times 10 \text{ mm}^3$ sample (Fig. 2b) was analyzed for decay time with three exponential decay functions, resulting in decay constants of $0.04 \mu\text{s}$ (3%), $0.17 \mu\text{s}$ (15%), and $0.47 \mu\text{s}$ (82%).

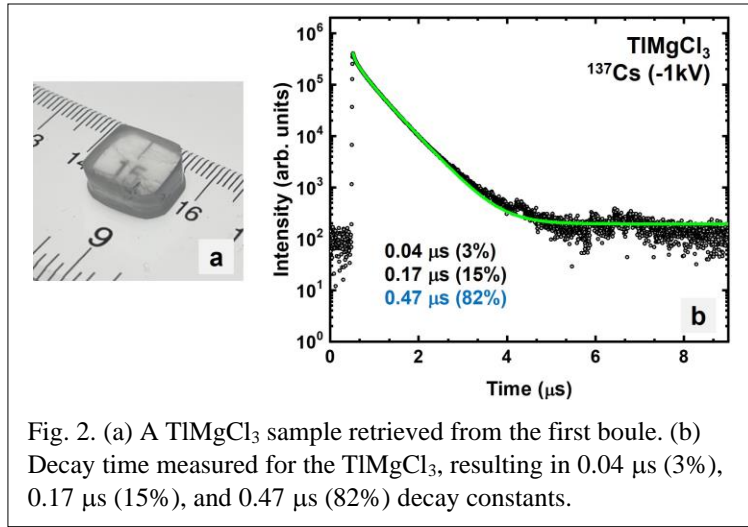


Fig. 2. (a) A TiMgCl_3 sample retrieved from the first boule. (b) Decay time measured for the TiMgCl_3 , resulting in $0.04 \mu\text{s}$ (3%), $0.17 \mu\text{s}$ (15%), and $0.47 \mu\text{s}$ (82%) decay constants.

^{137}Cs samples collected by other thin samples collected from along the growth direction of the first boule show a similar detection performance (energy resolution $\sim 4.6\%$ at FWHM for 662 keV), indicating that the boule was uniform (Fig. 3). Uniformity in the detector volume is important especially when an application requires that the entire detector volume be involved in detection.

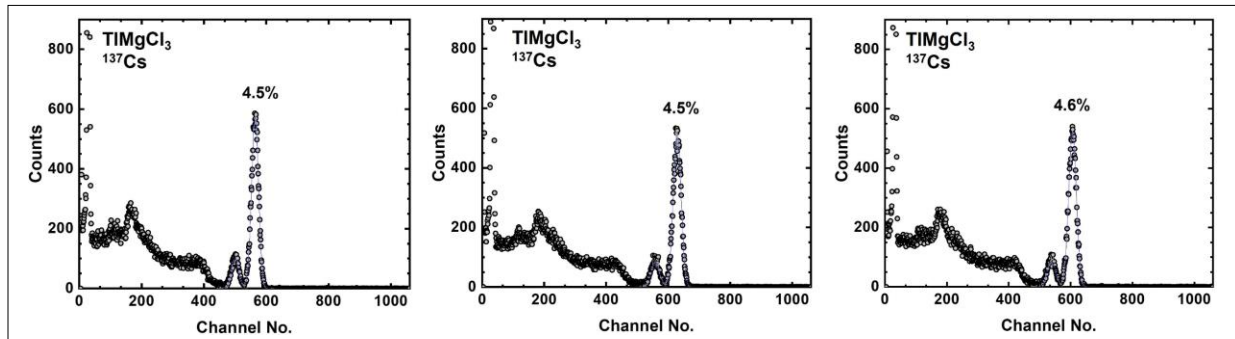
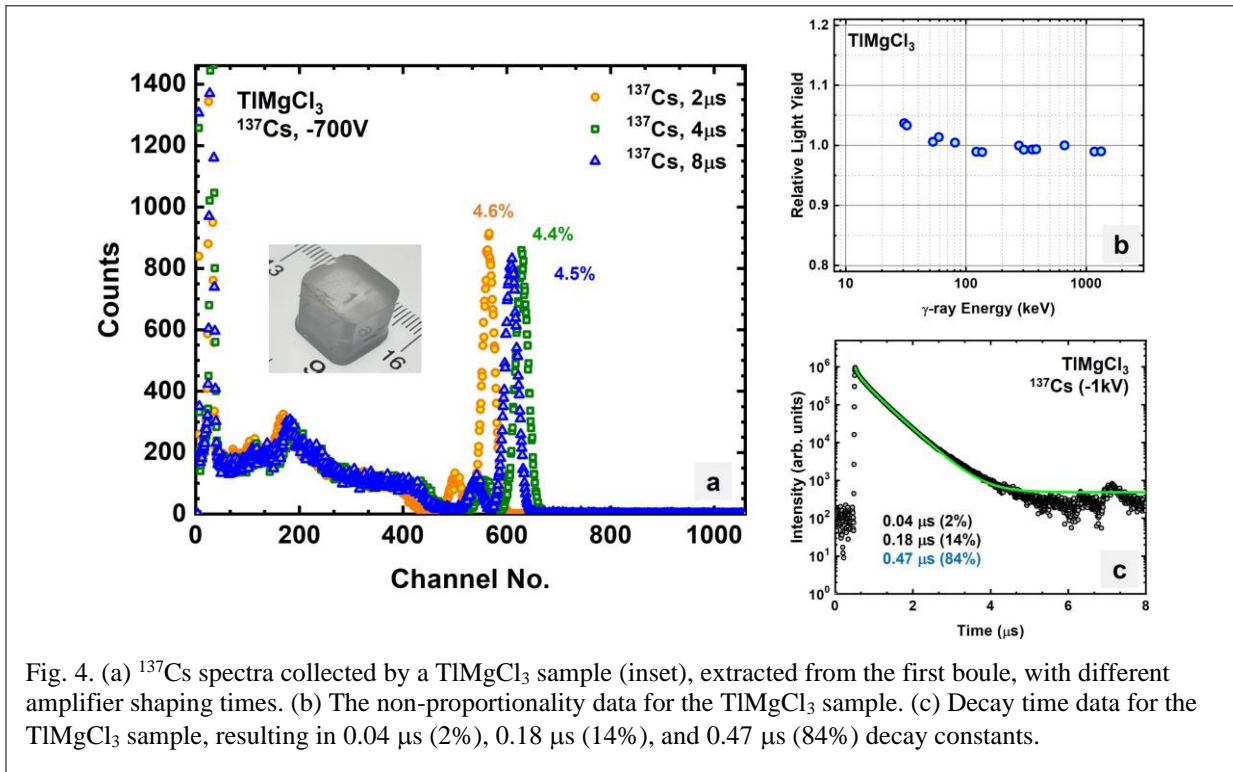
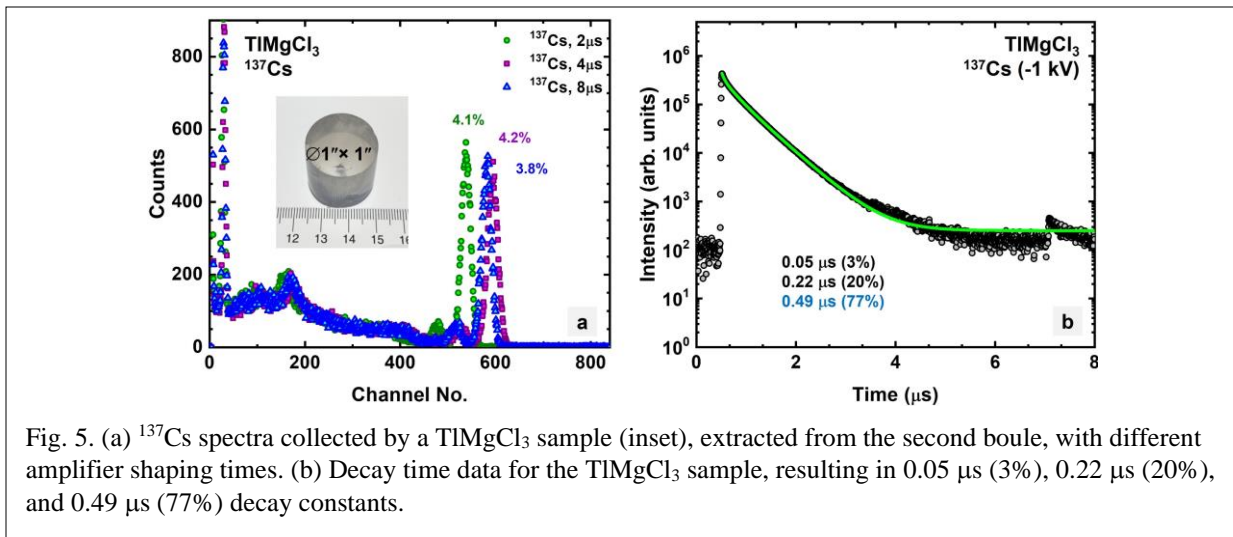


Fig. 3. ^{137}Cs spectra collected by samples extracted from the first TiMgCl_3 boule along the growth direction. The similarity of performance indicates a uniformly grown boule.

A thicker TiMgCl_3 crystal ($12 \times 15 \times 15 \text{ mm}^3$), also obtained from the first boule, collected ^{137}Cs spectra with different amplifier shaping time (Fig. 4a). Energy resolution of 4.4% (FWHM) at 662 keV was obtained for $4 \mu\text{s}$ shaping time. The non-proportionality data in Fig. 4b also shows that the response of TiMgCl_3 to γ -rays is linear for energy above 30 keV. The decay constants measured from the temporal profile in Fig. 4c are similar to the thinner TiMgCl_3 sample.



A bulk $\varnothing 1'' \times 1''$ TiMgCl_3 crystal collected ^{137}Cs spectra with different amplifier shaping times, resulting in a best energy resolution of 3.8% (FWHM) at 662 keV (Fig. 5a). This measurement was slightly better than the results obtained for the smaller crystals, which was probably due to better processing or the shape of the crystal (right cylinder vs. cuboid) that promotes better light collection, better processing (better polishing and no cracking or cleaving), and/or better crystal quality (lack of defects or imperfections). Further study on light collection in TiMgCl_3 may be needed. Similar decay time constants to the previous measurements for the smaller crystals were obtained when its temporal profile data was analyzed (Fig. 5b) TiCaCl_3



Small (16 mm) diameter

A section of an initial as grown Ø16-mm TlCaCl_3 crystal boule, using as received chemicals from vendors without purification, is shown in Fig. 6a. One of the roughly polished samples that were extracted by slicing the boule with a diamond wire saw and then later shaped into a rectangular cuboid ($12 \times 12 \times 10 \text{ mm}^3$) is shown in Fig. 6b.

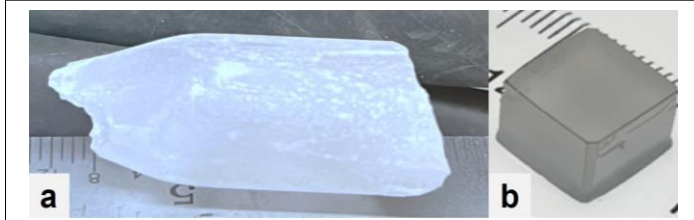


Fig. 6. (a) Ø 16-mm as grown TlCaCl_3 crystal boule, retrieved from cone-main section part of the grown boule. (b) Cut, lapped sample and as polished sample of TlCaCl_3 .

^{137}Cs spectra collected with the TlCaCl_3 crystal, with different amplifier shaping times, resulted in an energy resolution of 5.2% (FWHM) at 662 keV (Fig. 7a). Non-proportionality data in Fig. 7b shows that the response of TlCaCl_3 to γ -rays is linear for energy above 30 keV. Analysis on the temporal profile in Fig. 7c shows that the decay constants for TlCaCl_3 are 0.03 μs (1%), 0.28 μs (32%), and 0.69 μs (67%).

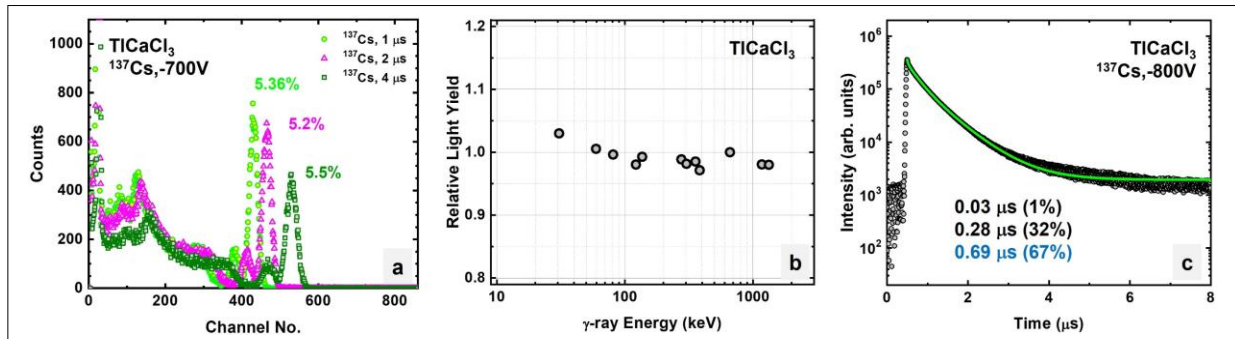
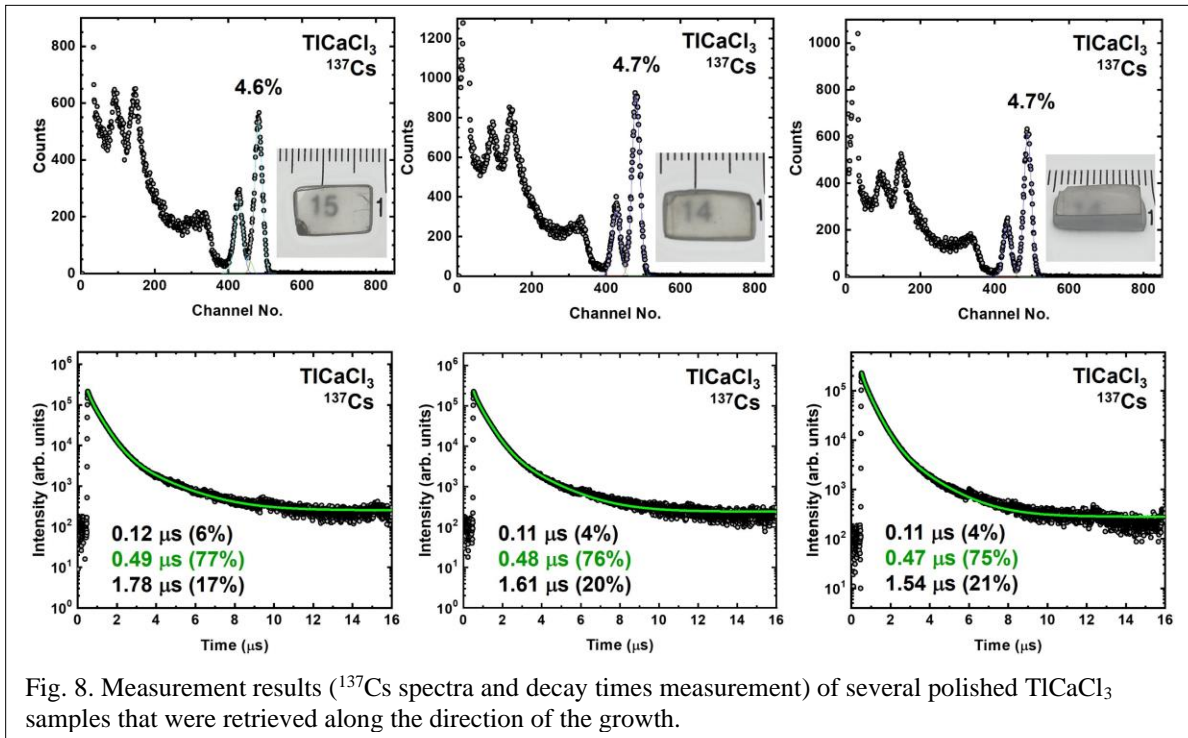


Fig. 7. (a) ^{137}Cs spectra collected by a TlCaCl_3 sample from Fig. 6 with different amplifier shaping times. (b) The non-proportionality data for the TlCaCl_3 sample. (c) Decay time data for the TlCaCl_3 sample, resulting in 0.03 μs (1%), 0.28 μs (32%), and 0.69 μs (67%) decay constants.

Fig. 8 shows the measurement results (^{137}Cs spectra and decay times measurement) of several polished TlCaCl_3 samples that were retrieved along the direction of the growth. The ^{137}Cs spectra shows similar energy resolution (approximately 4.6% FWHM at 662 keV) and similar full energy peak positions, which indicates that the boule was uniform in quality and performance.



One-inch diameter

An as grown bulk TiCaCl_3 single crack free crystal boule with an approximate length of 9.5 cm is shown in Fig. 9a. The outside of the boule was covered with a thin translucent layer that may have been organics or impurities due to excess of chloride reacting with the quartz ampoule. Under this translucent layer was a single crack free crystal, a sample of which was shown in Fig 9b before packaging. A sample cut from the boule was shaped into a rectangular cuboid (Fig. 9b) with the size of $16 \times 16 \times 25 \text{ mm}^3$, which was subsequently polished and hermetically encapsulated (Fig. 9c). The encapsulated crystal was characterized by collecting ^{137}Cs and ^{152}Eu spectra, as well as collecting the PMT anode signals to determine the temporal profile and determine decay time constants.

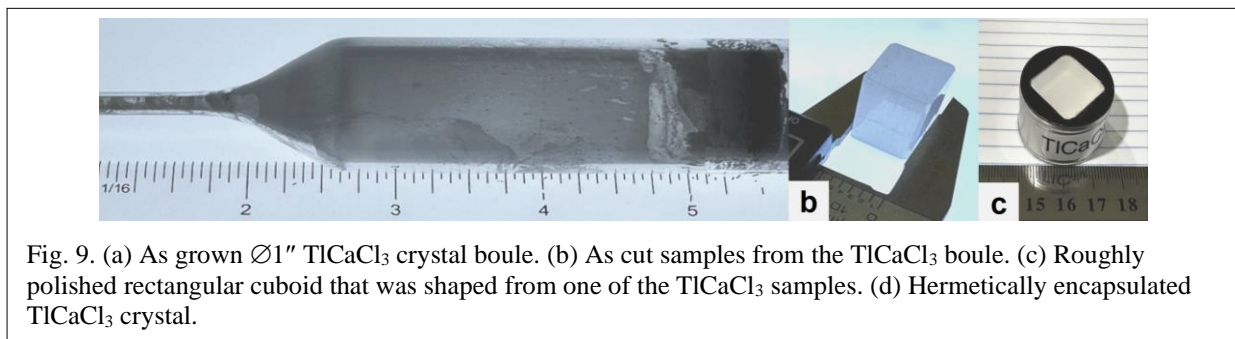
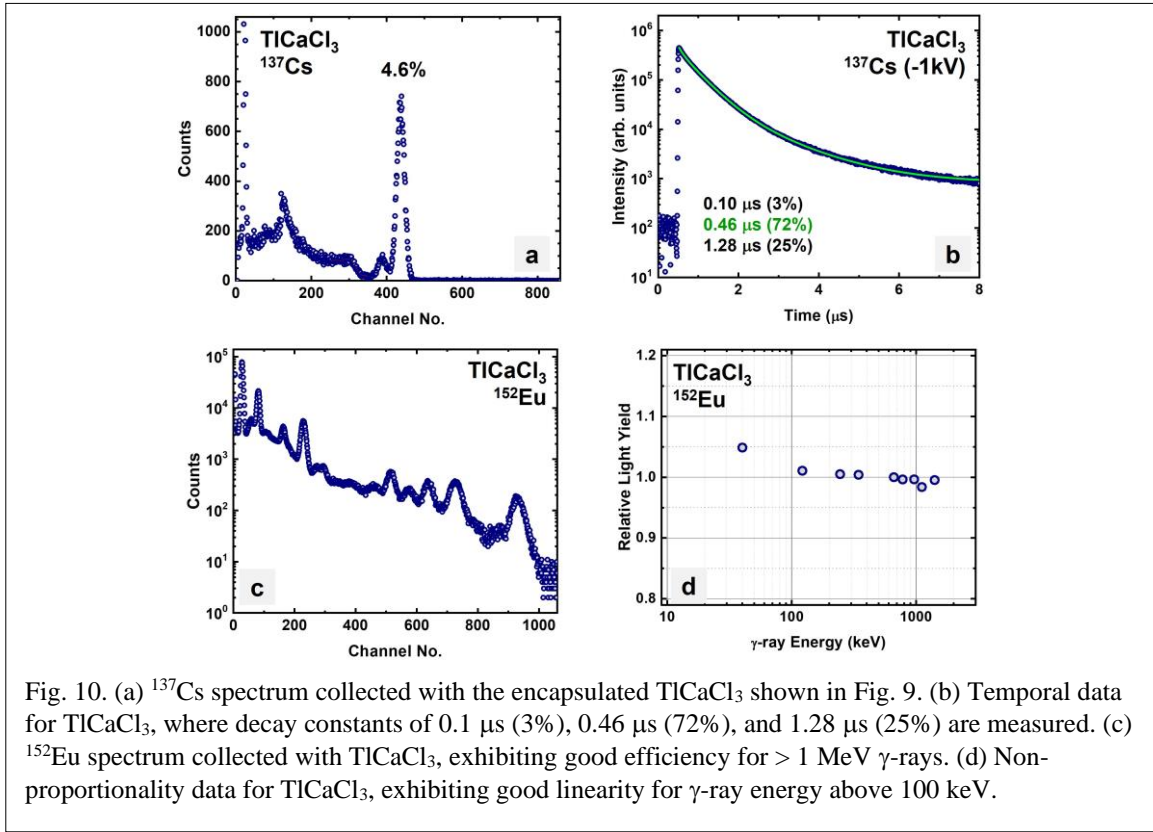


Fig. 10a shows the ^{137}Cs spectrum collected by the encapsulated TiCaCl_3 sample with measured 4.6% (FWHM) energy resolution at 662 keV. Decay constants of $0.1 \mu\text{s}$ (3%), $0.46 \mu\text{s}$ (72%), and $1.28 \mu\text{s}$ (25%) were measured (Fig. 10b). ^{152}Eu spectrum was also collected (Fig. 10c), from which the relative light yield data were calculated to determine the non-proportionality behavior of TiCaCl_3 (Fig. 10d). As in the case of the smaller sized TiCaCl_3 crystals, the crystal had a linear response to γ -rays with energy above 100 keV.



TiCaBr₃

Fig. 11a shows an as grown Ø14-mm TiCaBr₃ crystal boule with an approximate length of 7.5 cm. The visible crack in the mid-section of the boule was due to a power failure during the cooling process. ¹³⁷Cs spectra collected with different amplifier shaping times by a TiCaBr₃ sample are shown in Fig. 11b, with measured energy resolution of 5.3% (FWHM) at 662 keV. Comparison of ¹³⁷Cs spectra collected with a TiCaBr₃ sample from the Ø13×20-mm boule and a Ø1"×1" NaI:Tl is shown in Fig. 11c, showing that even with a smaller diameter, TiCaBr₃ exhibited a larger peak-to-Compton ratio than NaI:Tl. ¹⁵²Eu spectrum was also collected (Fig. 11d), from which the relative light yield data were calculated to determine the non-proportionality behavior of TiCaBr₃ (Fig. 11e). As in the case of other ternary TI-based halide crystals described so far, the crystal had a linear response to γ-rays with energy above 100 keV.

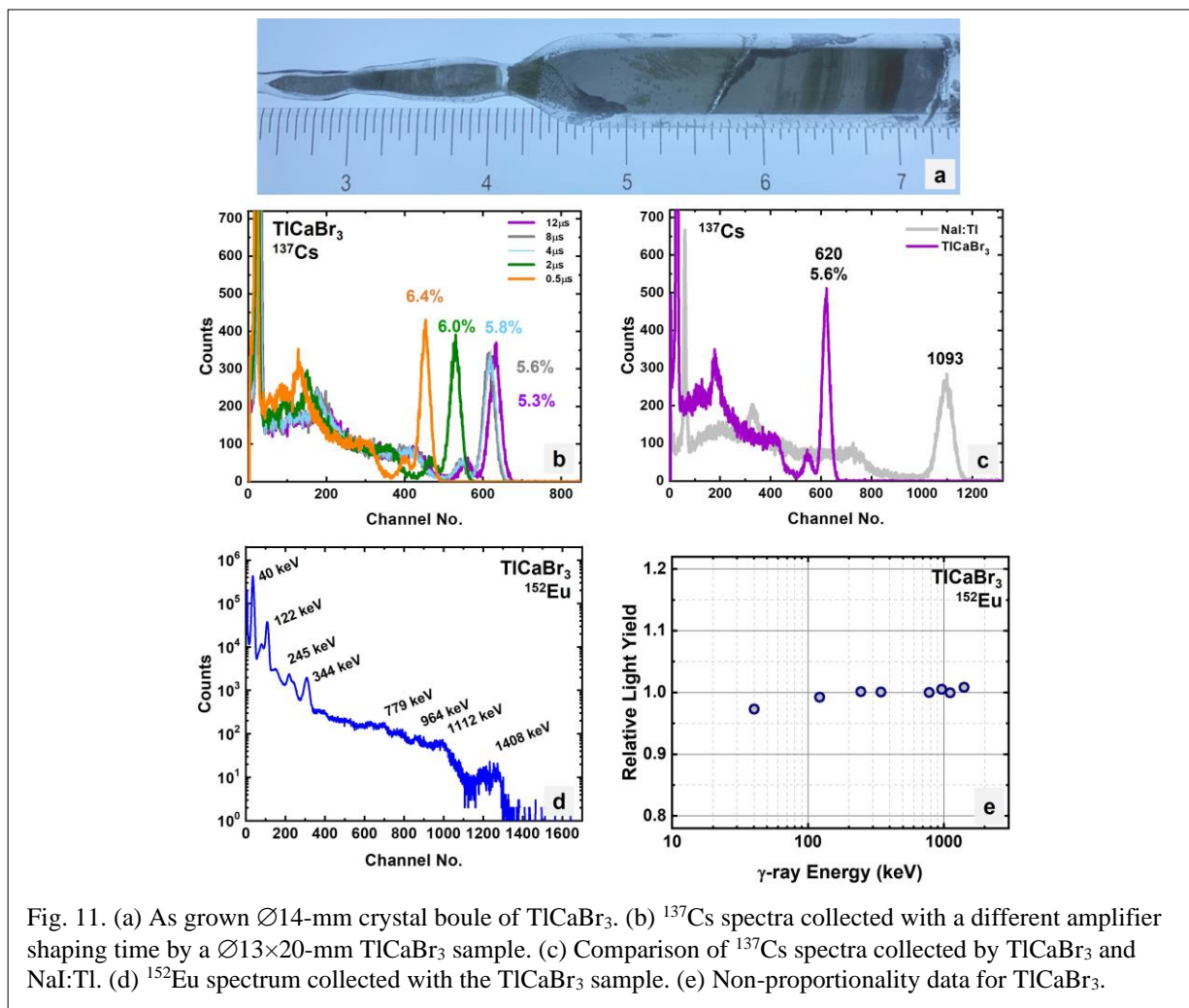


Fig. 11. (a) As grown Ø14-mm crystal boule of TICaBr₃. (b) ¹³⁷Cs spectra collected with a different amplifier shaping time by a Ø13×20-mm TICaBr₃ sample. (c) Comparison of ¹³⁷Cs spectra collected by TICaBr₃ and NaI:Tl. (d) ¹⁵²Eu spectrum collected with the TICaBr₃ sample. (e) Non-proportionality data for TICaBr₃.

Eu-doped TICa₂Br₅

Two as grown Ø16-mm crystal boules of TICa₂Br₅ (top: undoped, bottom: europium-doped) are shown in Fig. 12. The appearance of the crystals were not clear as one can observe from a processed thin sample of Eu-doped TICa₂Br₅ (inset picture in Fig. 13a), from which clearly there were more than one phases grown. A dopant (Eu²⁺) was used in attempt to improve scintillation properties like light yield, energy resolution, and decay time.

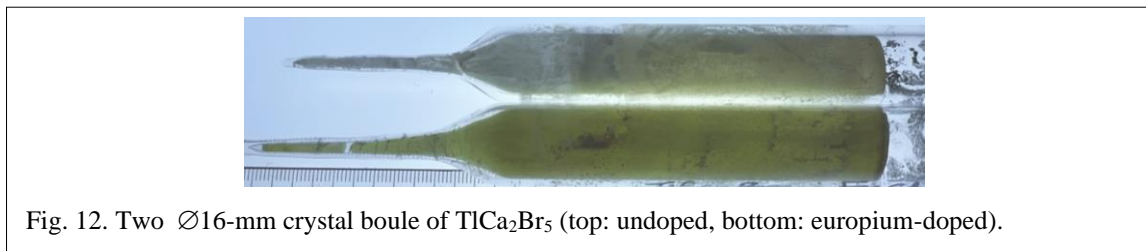


Fig. 12. Two Ø16-mm crystal boules of TICa₂Br₅ (top: undoped, bottom: europium-doped).

A sample extracted from $\text{TlCa}_2\text{Br}_5\text{:Eu}$ boule was characterized (Fig 13a inset). The crystal was not transparent and appeared to have more than one phases. Fig. 13a shows ^{137}Cs spectrum collected by the Eu-doped TlCa_2Br_5 crystal. Energy resolutions of 4.2% (FWHM at 662 keV) was measured.

Three decay constants were calculated (Fig. 13(b)): $0.54 \mu\text{s}$ (77%) and $1.8 \mu\text{s}$ (23%). According to the relative light yield vs. photon energy (non-proportionality) data (Fig. 13c), $\text{TlCa}_2\text{Br}_5\text{:Eu}$ has a relatively linear response ($\pm 0.05\%$) for a wide range of photon energy, especially for energy above 100 keV. Europium as a dopant appears to improve energy resolution and slightly improve light yield. However, crystal quality appears to have been compromised.

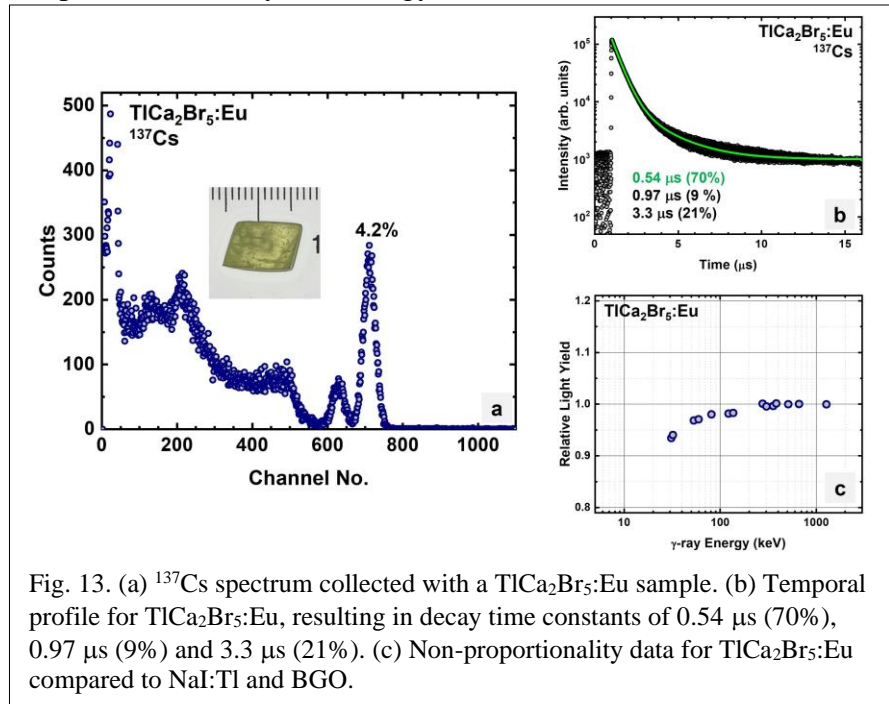


Fig. 13. (a) ^{137}Cs spectrum collected with a $\text{TlCa}_2\text{Br}_5\text{:Eu}$ sample. (b) Temporal profile for $\text{TlCa}_2\text{Br}_5\text{:Eu}$, resulting in decay time constants of $0.54 \mu\text{s}$ (70%), $0.97 \mu\text{s}$ (9%) and $3.3 \mu\text{s}$ (21%). (c) Non-proportionality data for $\text{TlCa}_2\text{Br}_5\text{:Eu}$ compared to NaI:Tl and BGO .

Mixed halide $\text{TlCa}(\text{Cl},\text{Br})_3$

As seen in the previous sections, for the thallium calcium halide system, there are several avenues that were attempted to improve the intrinsic and/or scintillation properties of the crystals. First, undoped TlCaBr_3 was grown as the base for comparison. Second, Eu-doped TlCa_2Br_5 was grown, resulting in slight improvement in light yield and energy resolution, while the crystal quality suffers. Third, (undoped) mixed halide $\text{TlCa}(\text{Cl},\text{Br})_3$ was grown. Fig. 14a shows ^{137}Cs spectra collected with different amplifier shaping times by a $\text{TlCa}(\text{Cl},\text{Br})_3$ sample.

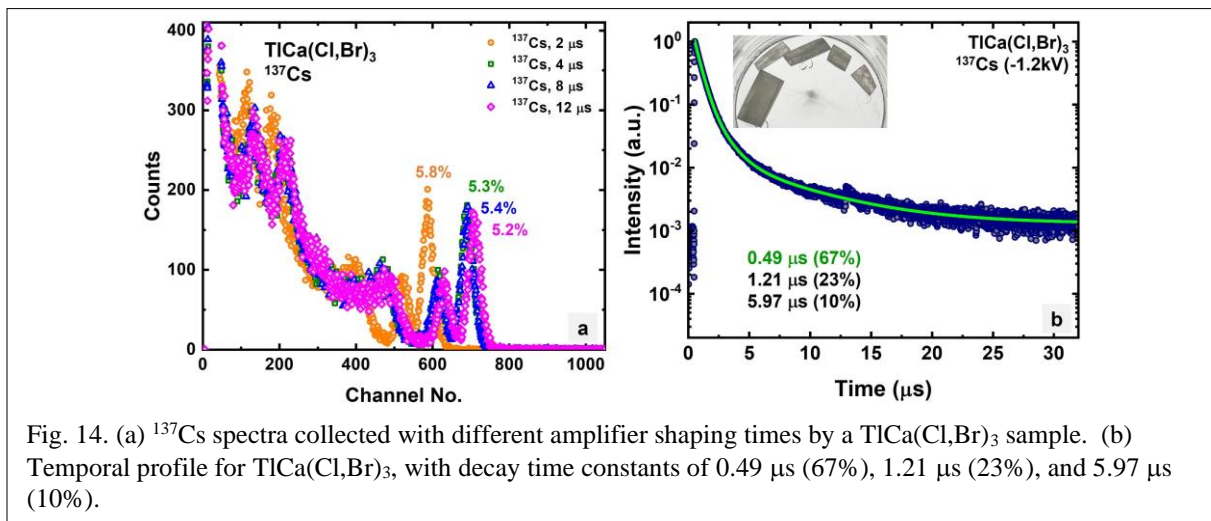


Fig. 14. (a) ^{137}Cs spectra collected with different amplifier shaping times by a $\text{TlCa}(\text{Cl},\text{Br})_3$ sample. (b) Temporal profile for $\text{TlCa}(\text{Cl},\text{Br})_3$, with decay time constants of $0.49 \mu\text{s}$ (67%), $1.21 \mu\text{s}$ (23%), and $5.97 \mu\text{s}$ (10%).

Compared to intrinsic TlCaBr_3 , no improvement was observed in either energy resolution or light yield. Fig. 14b shows the temporal profile for $\text{TlCa}(\text{Cl},\text{Br})_3$, with decay constants of $0.49 \mu\text{s}$ (67%), $1.21 \mu\text{s}$ (23%), and $5.97 \mu\text{s}$ (10%).

Eu-doped $\text{TlCa}(\text{Cl},\text{Br})_3$

Following the study presented in the previous sections, europium doped $\text{TlCa}(\text{Cl},\text{Br})_3$ were grown, with the results shown in Fig. 15. The crystals extracted from along the boule were not transparent, however, their performance was similar (energy resolution 5.5-5.8% (FWHM) at 662 keV; primary decay constant 0.50-0.58 μs), indicating that the boule was grown uniformly. There was no observable improvement to the energy resolution nor to the decay constants, as compared to TlCaBr_3 .

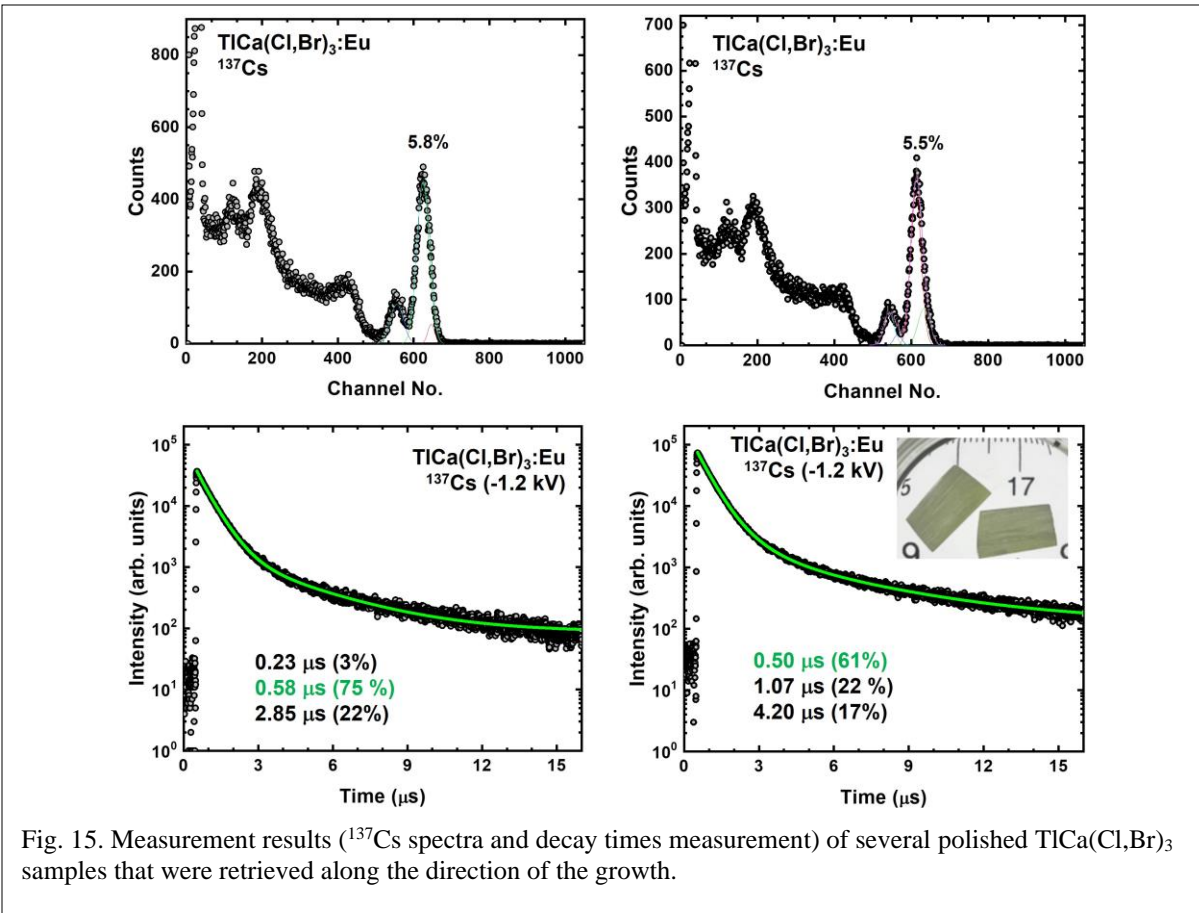


Fig. 15. Measurement results (^{137}Cs spectra and decay times measurement) of several polished $\text{TlCa}(\text{Cl},\text{Br})_3$ samples that were retrieved along the direction of the growth.

(Cs,Tl) $_3$ Cu $_2$ I $_5$

Initial $\varnothing 1''$ crystals of intrinsic $\text{Cs}_3\text{Cu}_2\text{I}_5$ and $\text{Cs}_3\text{Cu}_2\text{I}_5$ co-doped with Li^+ and Tl^+ were grown at XI, Inc. Fig. 16a shows ^{137}Cs spectra with different shaping times collected by a platelet like sample of intrinsic $\text{Cs}_3\text{Cu}_2\text{I}_5$ (inset picture), with energy resolutions of 4.8-5.1% (FWHM) at 662 keV were measured. Similar performance was obtained for $\text{Cs}_3\text{Cu}_2\text{I}_5$ co-doped with Li^+ and Tl^+ (Fig. 16b).

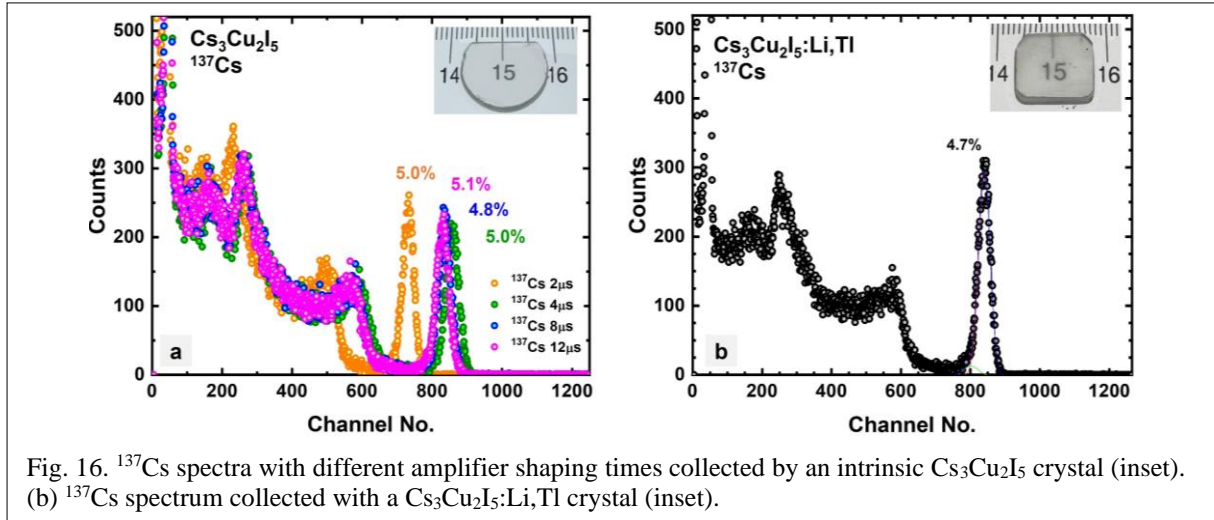


Fig. 16. ^{137}Cs spectra with different amplifier shaping times collected by an intrinsic $\text{Cs}_3\text{Cu}_2\text{I}_5$ crystal (inset). (b) ^{137}Cs spectrum collected with a $\text{Cs}_3\text{Cu}_2\text{I}_5:\text{Li,Tl}$ crystal (inset).

CONCLUSIONS

Table 3 summarizes the results and properties of ternary Tl-halide crystals successfully investigated and grown at XI, Inc. for imaging and high particle physics applications. These compounds have high Z_{eff} due to thallium and expected to have high physical densities. The best crystal quality and energy resolution (FWHM) at 662 keV were observed for intrinsic TlMgCl_3 . Additionally, TlMgCl_3 is not hygroscopic. The primary decay constants for these compounds are in the range of 0.45 to 0.55 μs . All of these compounds have proportional or linear response to γ -ray above 100 keV.

Table 3. Results and properties of ternary Tl-halide crystals grown

Compound	Z_{eff}	E_R	τ (μs)
TlMgCl_3	69.7	3.8%	0.47
TlCaCl_3	68.9	4.6%	0.47
TlCaBr_3	64.3	5.3%	0.49
TlCa(Cl,Br)_3	66.2	5.2%	0.49
$\text{TlCa}_2\text{Br}_5:\text{Eu}$	58.9	4.2%	0.52
$\text{TlCa(Cl,Br)}_3:\text{Eu}$	64.3	5.5%	0.50

ACKNOWLEDGMENT

This work was supported in part by the U.S. Department of Energy Grant No. DE-SC0022792.

REFERENCES

- [1] J.E. Brau, J.A. Jaros, H. Ma, "Advances in Calorimetry," *Annu. Rev. Nucl. Part. Sci.*, vol. 60, pp. 615–44 (2010).
- [2] <https://scintillator.lbl.gov/inorganic-scintillator-library>
- [3] R. Hawrami, E. Ariesanti, H. Wei, J. Finkelstein, J. Glodo, K.S. Shah, " $\text{Tl}_2\text{LaCl}_5:\text{Ce}$, high performance scintillator for gamma-ray detectors," *Nucl. Instrum. Meth. A*, vol. 869, pp. 107-109 (2017).
- [4] R. Hawrami, E. Ariesanti, H. Wei, J. Finkelstein, J. Glodo, K.S. Shah, "Intrinsic scintillators: TlMgCl_3 and TlCaI_3 ," *J. Cryst. Growth*, vol. 475, pp. 216-219 (2017).

- [5] R. Hawrami, E. Ariesanti, L. Soundara-Pandian, J. Glodo and K.S. Shah, "Tl₂LiYCl₆:Ce: A New Elpasolite Scintillator," *IEEE Trans. Nucl. Sci.*, vol. 63, no. 6, pp. 2838-2841 (2016).
- [6] R. Hawrami, E. Ariesanti, H. Wei, J. Finkelstein, J. Glodo, K. Shah, "Tl₂LiYCl₆: Large Diameter, High Performing Dual Mode Scintillator," *Crys. Growth Des.*, vol. 17, no.7, pp. 3960-3964 (2017).
- [7] H.J. Kim, G. Rooh, A. Khan, S. Kim, "New Tl₂LaBr₅: Ce³⁺ crystal scintillator for γ -rays detection," *Nucl. Instrum. Meth. A*, vol. 849, pp. 72-75 (2017).
- [8] R. Hawrami, E. Ariesanti, V. Buliga, A. Burger, "Thallium Strontium Iodide: Advanced Tl-Based Metal Halide Scintillator for Gamma-Ray Detection." Poster presented at the 2018 IEEE Nuclear Science Symposium (NSS) and Medical Imaging Conference (MIC), 10-17 Nov. 2018, Sydney, Australia.
- [9] R. Hawrami, E. Ariesanti, V. Buliga, A. Burger, "Thallium strontium iodide: A high efficiency scintillator for gamma-ray detection," *Opt. Mater.*, vol. 100, pp. 109624 (2020).
- [10] R. Hawrami, E. Ariesanti, A. Burger, H. Parkhe, "Latest updates in growth and performance of Ce-doped Tl₂LaCl₅ and Tl₂GdBr₅ and Eu-doped TlCa₂Br₅ and TlSr₂I₅," *Opt. Mater.*, vol. 121, pp. 111495 (2021).